

Macrosegregation in Dissimilar-Metal Fusion Welding

T. Soysal, S. Kou, D. Tat and T. Pasang

Abstract

Solute segregation on a macroscopic scale in a weld between two dissimilar metals or alloys has long been recognized, but fundamental understanding of macrosegregation in dissimilar-metal welding is still lacking. Two mechanisms for macrosegregation were proposed based on the liquidus temperature of the bulk weld metal, T_{LW} , relative to the liquidus temperature of metal 1, T_{L1} , and the liquidus temperature of metal 2, T_{L2} . According to the mechanisms, two distinctly different macrosegregation features can form. A “peninsula” of an unmixed metal 1 can form if $T_{LW} < T_{L1}$. On the other hand, a “beach” of unmixed metal 2 irregular in shape can form if $T_{LW} > T_{L2}$. To verify the mechanisms, a pure Cu sheet was butt welded to a low carbon steel sheet by gas-tungsten arc welding without a filler metal. Composition measurements were conducted inside and across the weld metal. A peninsula of unmixed steel and an irregular-shaped beach of unmixed Cu were observed, which verified the mechanisms. In addition, the bulk weld metal exhibited a layered structure caused by undercooling of the bulk weld pool into a metastable miscibility gap in the Cu-Fe phase diagram. Macroseggregation in previous studies on laser- and electron-beam welding of Cu to steel or stainless steel was discussed in light of the findings in the present study.

T. Soysal and S. Kou are respectively Graduate Student and Professor in the Department of Materials Science and Engineering, the University of Wisconsin, Madison, WI 53706. D. Tat and T. Pasang are respectively Undergraduate Student and Professor in the Department of Mechanical Engineering, Auckland University of Technology, Auckland, New Zealand.

1
2
3
4 **Introduction**
5
6

7
8 Dissimilar-metal welding, that is, welding two different metals or alloys together, has
9
10 been an area of active research. Usually, dissimilar-metal fusion welding is feasible unless
11
12 massive brittle intermetallic compounds form during solidification to cause severe cracking in
13
14 the resultant weld metal, i.e., the fusion zone. Two examples of feasible dissimilar-metal fusion
15
16 welding are well known, i.e., welding Cu to steel [1-5] or stainless steel [6-10], and welding
17
18 stainless steel to steel or Ni-base alloys [11-14]. The first example is related to heat exchangers,
19
20 where Cu tubes can enhance heat exchange because of their excellent thermal conductivity. The
21
22 second example is related to power plants, where stainless steels or Ni-base alloys can offer
23
24 superior corrosion resistance.
25
26
27

28
29 In dissimilar-metal welding, solute segregation on the macroscopic scale across the weld
30
31 metal, called macrosegregation hereinafter, can occur because of the inherent composition
32
33 difference between the two metals or alloys that are welded together. In addition to composition
34
35 variations, features distinctly different from their surrounding bulk weld metal in microstructure
36
37 as well as composition often exist near the fusion boundary and sometimes even far away from
38
39 it. The features are much closer (in fact, often identical) to the base metals in composition than
40
41 the surrounding weld metal.
42
43
44

45
46 Macrosegregation features such as base-metal-like “beaches”, “peninsulas” and “islands”
47
48 have been reported. Doody [11] welded carbon steel to stainless steel. The words “beach” and
49
50 “island” were used for the first time to describe macrosegregation features. He observed base-
51
52 metal-like beaches and islands on the carbon steel side of the weld. Omar [12] also welded
53
54 carbon steel to stainless steel and observed beaches, peninsulas and islands on the carbon-steel
55
56 side. The formation of these macrosegregation features was not understood.
57
58
59
60

1
2
3
4 Macroseggregation occurs not only in dissimilar-metal welding but also in dissimilar-filler
5
6 welding, that is, welding with a filler metal different from the workpiece in composition.
7
8 Macroseggregation features have been reported to cause problems such as loss of toughness [8],
9
10 hydrogen cracking [15-17], corrosion [18, 19] and stress-corrosion cracking [11, 18, 20, 21].
11
12 Thus, it is essential to understand how macroseggregation forms in welds.
13
14

15
16 Savage and coworkers [22, 23] first discovered macroseggregation near the fusion
17
18 boundary in dissimilar-filler welding. An “unmixed zone” was found near the fusion boundary,
19
20 that is, a beach. It was explained that a stagnant or laminar-flow layer of liquid base metal can
21
22 exist at the pool boundary and solidify, without mixing with the bulk weld pool. Due to the
23
24 viscosity of liquid metals, fluid flow in the weld pool diminishes near the pool boundary, where
25
26 the fluid velocity becomes zero, that is, the so-called no-slip boundary condition in fluid
27
28 mechanics [24]. Consequently, even though two melted base metals can be thoroughly mixed to
29
30 become an essentially homogeneous bulk weld pool, a thin layer of melted but unmixed base
31
32 metal may still exist near each pool boundary. Peninsulas, called “folds”, were also observed but
33
34 not explained [22, 23]. More recently, Kou and Yang [25-30] proposed two mechanisms for the
35
36 formation of macroseggregation features in dissimilar-filler welding, based on the liquidus
37
38 temperature of the base metal T_{LB} and that of the weld metal T_{LW} . A peninsula or island of the
39
40 base metal composition can form if $T_{LW} < T_{LB}$ while an irregular-shaped beach of the base metal
41
42 composition can form if $T_{LW} > T_{LB}$. Both mechanisms were verified in numerous experiments,
43
44 including welding Al alloys with various Al filler metals and welding Cu with Cu filler metals of
45
46 various Ni contents.
47
48
49
50
51
52
53
54

55 In the present study mechanisms for macroseggregation in dissimilar-metal welding will
56
57 be proposed based on the concepts behind the macroseggregation mechanisms of Kou and Yang
58
59
60
61
62
63
64
65

1
2
3
4 [25-30] for dissimilar-filler welding. To help subsequent discussion, these concepts are first
5
6 illustrated in Fig. 1 for the welding of a base metal of liquidus temperature T_{LB} . Fig. 1a shows the
7
8 case of welding without a filler metal. The entire pool boundary is an isotherm at T_{LB} including
9
10 the solidification front (that is, the trailing portion of the pool boundary) if undercooling is
11
12 negligible. The resultant weld metal is macroscopically uniform in composition (but
13
14 microsegregation still exists).
15
16

17
18
19 When a dissimilar filler metal is used, it is well mixed in the bulk weld pool. Houldcroft
20
21 [31] showed in dissimilar-filler welding that the bulk weld metal is uniform in composition due
22
23 to vigorous mixing in the weld pool. Examples of driving forces for mixing include the Lorentz
24
25 force and surface-tension gradients along the pool surface [32, 33]. Fig. 1b shows the case where
26
27 the composition of the filler metal changes the composition of the bulk weld pool (and hence the
28
29 composition of the bulk weld metal) such that the liquidus temperature of the bulk weld metal is
30
31 no longer at T_{LB} but reduced to T_{LW} , that is, $T_{LW} < T_{LB}$. Thus, the solidification front of the bulk
32
33 weld pool shifts backward from T_{LB} to T_{LW} . This is because, according to heat flow in welding
34
35 [34], a lower-temperature isotherm is located farther away from the heat source than a higher-
36
37 temperature one. Thus, the weld pool boundary is no longer isothermal at T_{LB} .
38
39
40
41
42

43
44 As illustrated in Fig. 1b, due to diminishing fluid flow near the pool boundary, a layer of
45
46 unmixed liquid base metal can exist along the pool boundary, that is, a layer of melted base
47
48 metal not mixed with the bulk weld pool. The thickness of the layer is exaggerated for clarity of
49
50 illustration. Since the layer has the same composition as the base metal, it solidifies as a beach of
51
52 the base metal composition. Thus, the resultant weld metal is no longer uniform in composition.
53
54 The region of the bulk weld pool ahead of the solidification front is below T_{LB} , that is, cooler
55
56 than the temperature at which liquid base metal can start freezing. Thus, if convection carries the
57
58
59
60
61
62
63
64
65

1
2
3
4 melted but unmixed base metal into the cooler bulk weld pool near the solidification front, it can
5
6 start freezing quickly in to a base-metal-like peninsula or island before it has time to mix with
7
8 the surrounding bulk weld pool. This can explain why a base-metal-like peninsula can form in
9
10 the bulk weld pool without mixing with it. Further information is available elsewhere [25-30].
11
12

13
14 Contrarily, as shown in Fig. 1c, the filler metal changes the composition of the bulk weld
15
16 pool (and hence the composition of the bulk weld metal) such that the liquidus temperature of the
17
18 bulk weld metal is no longer at T_{LB} but raised to T_{LW} , that is, $T_{LW} > T_{LB}$. Thus, the solidification
19
20 front of the bulk weld pool shifts forward from T_{LB} to T_{LW} . Again, the layer of unmixed liquid
21
22 base metal solidifies as a beach of the base metal composition. The layer is below T_{LW} , that is,
23
24 cooler than the temperature at which the bulk weld pool can start freezing. Thus, if convection
25
26 pushes the liquid in the bulk weld pool into this cooler layer, it can start freezing quickly as
27
28 weld-metal intrusions before it has time to mix with the liquid base metal. The liquid base metal
29
30 still inside the liquid layer subsequently solidifies as a base-metal-like beach of irregular shape.
31
32 This can explain why melted base metal in the layer can solidify without mixing with the bulk
33
34 weld pool and appear highly irregular in shape. Again, further information is available elsewhere
35
36 [25-30].
37
38
39
40
41
42

43 **Experimental procedure**

44
45 To focus on the fundamental understanding of macrosegregation in dissimilar-metal
46
47 welding, Cu and steel were selected for welding because the weld metal is essentially a simple
48
49 binary Cu-Fe alloy that can be studied based on the binary Cu-Fe phase diagram. The Cu was a
50
51 commercially pure Cu (Grade 110: Cu = 99%; O = 0.04% and trace amount of Ag) and the steel
52
53 a low carbon steel, both 1.2 mm thick, 60 mm wide and 150 mm long.
54
55
56
57
58
59
60
61
62
63
64
65

1
2
3
4 Gas-tungsten arc welding (GTAW), which is also called tungsten-inert gas (TIG)
5
6 welding, was selected for the present study. Dissimilar-metal welding of Cu to steel, stainless
7
8 steel or pure Fe has been studied by GTAW [10] and by laser- or electron-beam welding [1, 2, 4-
9
10 10]. GTAW was selected because fluid flow in the weld pool is simpler, more stable and better
11
12 understood in GTAW [32, 33] than in laser- or electron-beam welding. In laser- and electron-
13
14 beam welding with a keyhole, the interactions between the vapor pressure, surface tension and
15
16 gravity can make fluid flow highly unstable and complex. This can make macrosegregation in
17
18 dissimilar-metal welding more difficult to understand. Also, unlike laser- or electron-beam
19
20 welding, GTAW is readily accessible. It is of practical interest if dissimilar-metal welds can be
21
22 made cost effectively.
23
24
25
26
27

28
29 Butt welding by GTAW was conducted, without a filler metal, in the length direction
30
31 along the joint with a 1.5 mm offset of the electrode tip into the Cu side. The welding conditions
32
33 were as follows: DC electrode negative (straight polarity), 60 A current, 9.5 V voltage, 1 mm/s
34
35 travel speed, and 11 L/min Ar flow rate. Welding was conducted manually at the travel speed of
36
37 about 1 mm/s, with the electrode tip pointed forward in the welding direction and without
38
39 circular or back-and-forth movement of the torch. Forward welding is common in GTAW,
40
41 typically with an angle of 60 to 70° between the electrode and the workpiece. The back side of
42
43 the workpiece was protected by Ar by mounting the workpiece on a purge box.
44
45
46
47

48
49 The resultant weld was cut normal to the welding direction and polished. The macrograph
50
51 of the weld was taken after etching it with an acid chloride solution consisting of 20 ml
52
53 hydrochloric acid (HCl), 5g ferric chloride (FeCl₃) and 100 ml H₂O. It was found that the
54
55 etching solution dissolved Fe excessively, leaving the Fe-rich phase (dendrites and particles) as
56
57 deep grooves or pits after etching. Thus, for the composition measurements by electron probe
58
59
60
61
62
63
64
65

1
2
3
4 microanalysis (EPMA), the weld was re-polished but not etched. As for scanning electron
5
6 microscopy (SEM), the weld was etched with 3 % Nital. Under SEM, the Fe-rich phase appeared
7
8 flat and just slightly below the surface of the Cu-rich phase, not as deep grooves or pits. Some
9
10 composition measurements were also conducted by energy dispersive spectroscopy (EDS) on
11
12 SEM.
13
14

15
16 EPMA was performed with a CAMECA SX51 electron probe, operating at 15 kV and 15
17
18 nA, with a 25 micron defocused beam, using LIF crystals and P10 gas flow proportional
19
20 detectors. Counting times were 10 seconds on peak and 10 seconds on backgrounds, with
21
22 minimal detection limits of 0.04 wt% for both Cu and Fe. Pure Fe and Cu were used as
23
24 standards. Matrix corrections were performed with Probe for EPMA software using the PAP
25
26 algorithm. Composition measurements were made at selected points in the weld. To measure the
27
28 local average composition at a point, four measurements were made right next to each other to
29
30 cover a square area of 50 microns by 50 microns, plus one additional measurement at the center
31
32 of the square. The average of the five measurements was taken as the local average composition
33
34 at the point of composition measurement. In addition to selected points, composition
35
36 measurements also were made along a straight line across the entire weld at an interval of 100
37
38 microns.
39
40
41
42
43
44

45 46 **Results and Discussion**

47
48 Two mechanisms for macrosegregation in dissimilar-metal welding will be proposed as
49
50 follows based on the liquidus temperature of the bulk weld metal T_{LW} relative to the liquidus
51
52 temperature of metal 1 (or alloy 1) T_{L1} and the liquidus temperature of metal 2 (or alloy 2) T_{L2} .
53
54 For the purpose of discussion, steel will be considered as metal 1 and Cu metal 2.
55
56
57
58

59 60 **1. Mechanism I**

1
2
3
4 Figure 2 shows Mechanism I for the case of $T_{LW} < T_{LI}$. It is illustrated using the Cu-Fe
5
6 binary phase diagram in Fig. 2a as an example. T_{LW} is based on the measured composition of the
7
8 bulk weld metal, which will be shown subsequently in Fig. 5. The plan view of the weld pool is
9
10 shown in Fig. 2b. As explained previously in Fig. 1, when the bulk weld pool and the base metal
11
12 differ from each other in composition, the pool boundary is no longer isothermal at the liquidus
13
14 temperature of the base metal. As illustrated in Fig. 2c, the solidification front of the bulk weld
15
16 pool is at T_{LW} and that of the layer of unmixed liquid metal 1 is at T_{LI} . When undisturbed by
17
18 convection, this layer can begin to solidify at T_{LI} into a beach of base metal 1. As mentioned
19
20 previously, a lower-temperature isotherm should be located farther behind the heat source than a
21
22 higher-temperature one. Thus, since $T_{LW} < T_{LI}$, the solidification front of the bulk weld pool T_{LW}
23
24 is shifted backward to behind isotherm T_{LI} .
25
26
27
28
29

30
31 As shown in Fig. 2c, the region of the bulk weld pool ahead of the solidification front is
32
33 cooler than T_{LI} , that is, cooler than the temperature at which the liquid metal 1 can start freezing.
34
35 Thus, as shown in Fig. 2d, when carried backward from the layer of unmixed liquid metal 1 into
36
37 the cooler region of the bulk weld pool ahead of the solidification front, liquid metal 1 can start
38
39 to freeze quickly before significant mixing with the surrounding liquid. Since the two liquids are
40
41 in intimate contact with each other, heat transfer between them is highly effective and thus able
42
43 to cool liquid metal 1 immediately. Consequently, a peninsula and even an island of metal 1 can
44
45 form.
46
47
48
49

50
51 It should be noted that fluid flow needs not to be exactly in a horizontal plane in order to
52
53 form a peninsula. However, it does need to have a component in the backward direction
54
55 (opposite to the welding direction) in order to be able to carry liquid metal 1 into the cooler
56
57 region of the bulk weld pool ahead of the solidification front. This is because, if liquid base
58
59
60
61
62
63
64
65

1
2
3
4 metal 1 is carried forward (in the welding direction) into the bulk weld pool, it will be
5
6 superheated and thus cannot freeze quickly as a peninsula of unmixed metal 1 (maybe possible
7
8 as a partially mixed peninsula). Consequently, peninsulas of unmixed metal 1 do not form
9
10 everywhere along the fusion boundary and may not show up in a weld cross-section taken at a
11
12 random location along the weld even when they do exist inside the weld. It should also be noted
13
14 that if the tail of a peninsula is cut normal to the weld, it may appear as an island instead of a
15
16 peninsula.
17
18
19
20
21

22 **2. Mechanism II**

23
24 Figure 3 shows Mechanism II for the case of $T_{LW} > T_{L2}$. Again, it is illustrated using the
25
26 Cu-Fe binary phase diagram as an example, as shown in Fig. 3a. The plan view of the weld pool
27
28 is shown in Fig. 3b. Again, the pool boundary is not isothermal as shown in Fig. 3c. The bulk
29
30 weld pool begins to solidify at T_{LW} (or lower if undercooling occurs) and the layer of unmixed
31
32 liquid metal 2 begins to solidify at T_{L2} . When undisturbed by convection, this layer can solidify
33
34 into a beach of base metal 2.
35
36
37

38
39 The effect of convection on macrosegregation is explained in Fig. 3d. The layer of
40
41 unmixed liquid metal 2 is cooler than T_{LW} , that is, cooler than the temperature at which the bulk
42
43 weld pool can start freezing, as already shown in Fig. 3c. Thus, when the liquid in the bulk weld
44
45 pool is pushed by convection into this layer, it can start to freeze quickly as intrusions of the bulk
46
47 weld metal. When the layer of unmixed liquid metal 2 is intruded, some liquid metal 2 can
48
49 remain in the layer and some gets pushed out into the bulk weld pool. The unmixed liquid metal
50
51 2 remaining in the layer can subsequently solidify as a beach of metal 2 that is irregular in shape.
52
53 Since the liquid metal 2 pushed out of the layer into the bulk weld pool is superheated above its
54
55 liquidus temperature T_{L2} , it cannot solidify right away. So, it has time to mix with the bulk weld
56
57
58
59
60
61
62
63
64
65

1
2
3
4 pool to become partially mixed metal 2 near the irregular beach of unmixed metal 2, or even
5
6 carried away into the bulk weld pool to become partially mixed islands of metal 2. If $T_{LW} \gg T_{L2}$,
7
8 the following features are likely to exist: a thick beach of unmixed metal 2, a thick layer of
9
10 partially mixed metal 2 near the beach, and large islands of partially mixed metal 2.
11
12
13

14 It is perhaps worth pointing out that irregular-shaped beaches caused by Mechanism II
15
16 are much easier to find in welds than peninsulas caused by Mechanism I. This is because any
17
18 fluid flow toward the weld pool boundary can result in an irregular-shaped beach. Surface-
19
20 tension gradients along the weld pool surface, for instance, are known to induce surface flow
21
22 toward the pool edge [34], which can easily turn toward the pool boundary.
23
24
25

26 27 **3. Verification of Mechanisms I and II**

28
29 Figure 4 shows optical images taken from the transverse cross-section of a butt weld
30
31 made between pure Cu and low carbon steel. The weld specimen was etched with the acid
32
33 chloride solution mentioned previously. The transverse macrograph in Fig. 4a shows the overall
34
35 structure of the weld, in which the welding direction is normal to and upward from the
36
37 macrograph. The dotted lines indicate the fusion boundaries. Three macrosegregation features in
38
39 the fusion zone can be seen: (i) a peninsula on the steel side, (ii) an irregular-shaped beach on the
40
41 Cu side, and (iii) a layered macrostructure in the bulk weld metal, which is a special case for Cu-
42
43 to-steel welding and thus will be discussed separately subsequently. In Fig. 4b the fusion
44
45 boundary on the Cu side is revealed by heavy etching. Epitaxial growth of grains from the Cu
46
47 base metal into the fusion zone is evident [34]. Along the upper part of the fusion boundary on
48
49 the steel side, a thin beach about 30 μm thick can still be seen at higher magnifications. Before
50
51 the liquid steel was carried away by convection to form the peninsula, the beach could have been
52
53 thicker.
54
55
56
57
58
59
60
61
62
63
64
65

1
2
3
4 It is worth pointing out that in the previous studies by one of the authors (Kou) on
5
6 dissimilar-filler welding [25, 29], a partially penetrating weld was made on a single plate (a
7
8 bead-on-plate weld) with a dissimilar filler metal. Macrographs were taken from the vertical
9
10 longitudinal cross-section along the weld central plane. Peninsulas were observed near the fusion
11
12 boundary and they always pointed in the opposite direction of welding as suggested by the
13
14 mechanism proposed for the formation of peninsulas. However, for the fully penetrating butt
15
16 weld in the present study a similar vertical longitudinal macrograph does not help because the
17
18 weld bottom does not even have a fusion boundary to allow a peninsula to form. Thus, a
19
20 transverse macrograph such as that in Fig. 4a is preferred because it at least shows that a
21
22 peninsula exists.
23
24
25
26
27

28 Fig. 4c shows the microstructure of the peninsula and its surrounding bulk weld metal.
29
30 Low carbon steel typically does not exhibit a solidification microstructure, neither dendrites nor
31
32 cells. This is probably because of its very low alloying elements, fast carbon diffusion, and post-
33
34 solidification phase transformations. Thus, it is not surprising that the peninsula does not have a
35
36 solidification microstructure to directly confirm that it originated from solidification of a liquid
37
38 alloy. However, a solid chunk broken off by convection from the steel side that remained
39
40 unmelted during welding could not possibly have the smooth shape of the peninsula. The
41
42 numerous dendrites that grow from the peninsula indicate that the melted steel solidified before
43
44 the surrounding bulk weld pool did. This confirms $T_{LW} < T_{LI}$.
45
46
47
48
49

50 The results of composition measurements by EPMA are shown in Fig. 5, including the
51
52 point composition measurements at selected points in the weld metal and the line composition
53
54 measurements across the entire weld metal. The vertical dotted lines 1 through 8 indicate where
55
56 the line of composition measurements intersects various boundaries in the microstructure. A Fe-
57
58
59
60
61
62
63
64
65

1
2
3
4 rich layer, between line 7 and 8, exists near the steel-side of the fusion zone. The rest of the
5
6
7 fusion zone is essentially Cu-rich, which is consistent with the more Cu than steel in the fusion
8
9
10 zone, caused by the 1.5 mm offset of the electrode tip into the Cu side and the much lower
11
12 melting point of Cu than steel. The Fe-content profile shows a few peaks, e.g., those indicated by
13
14 lines 3, 4 and 5.

15
16 As shown by point composition measurements, the peninsula contains Fe and no Cu, that
17
18 is, it is steel, unmixed with the surrounding bulk weld metal. This suggests that during welding
19
20 the melted steel was carried into the adjacent bulk weld pool, which was cooler than the liquidus
21
22 temperature of steel T_{LI} and thus caused the liquid steel to freeze quickly before mixing with the
23
24 bulk weld pool. As shown by point composition measurements, the bulk weld metal surrounding
25
26 the peninsula has a Fe content of about 30 to 35 wt%. According to the Cu-Fe phase diagram in
27
28 Fig. 2a, this composition corresponds to a liquidus temperature of about 1425°C, that is, the
29
30 liquidus temperature of the bulk weld metal surrounding the peninsula T_{LW} is 1425°C. Since low
31
32 carbon steel is close to pure Fe in composition, the liquidus temperature of low carbon steel can
33
34 be taken as the melting point of pure Fe as an approximation, that is, $T_{LI} = 1538^\circ\text{C}$. Thus, the
35
36 condition of $T_{LW} < T_{LI}$ for Mechanism I to occur on the steel side of the fusion boundary is
37
38 verified.
39
40
41
42
43
44

45 The composition measurements also identify the existence of an irregular beach of Cu,
46
47 unmixed with the surrounding bulk weld metal. The line composition measurements between
48
49 vertical dotted lines 1 and 2 show a pure Cu beach. The point measurement inside the beach also
50
51 confirms the beach is pure Cu.
52
53

54 As shown by the line composition measurements across the weld, the Fe content of the
55
56 bulk weld metal ranges from about 22 to 50%. Thus, according to the phase diagram in Fig. 3a,
57
58
59
60
61
62
63
64
65

1
2
3
4 the liquidus temperature of the bulk weld metal T_{LW} is about 1411 to 1433°C. In Fig. 3a (and in
5
6 Fig. 2a) this range of T_{LW} is highlighted in gray between two vertical arrowheads. Since the
7
8 melting point of pure Cu (metal 2) is 1085°C, $T_{L2} = 1085^\circ\text{C}$. Thus, the condition of $T_{LW} > T_{L2}$ for
9
10 Mechanism II to occur on the Cu side is also verified. As will be shown subsequently, the
11
12 solidification microstructure inside the intruded region of the beach is much finer than that in the
13
14 nearby bulk weld metal. This suggests quick freezing of the bulk weld pool occurred when it was
15
16 pushed into the cooler liquid Cu layer, consistent with Mechanism II.
17
18
19
20

21 It is interesting to note that the layer of liquid Cu along the pool boundary is very thick.
22
23 Based on Fig. 4b, the average thickness of the upper portion of the unmixed-Cu is about 150 μm .
24
25 The lower portion appears even thicker, and this is likely because Cu tends to sink in view of the
26
27 higher density of Cu (8.96 g/cc) than Fe (7.86 g/cc). Two factors could have contributed to the
28
29 very thick layer of the unmixed liquid Cu. First, $T_{LW} \gg T_{L2}$. The melting point of Cu, T_{L2} , is
30
31 1085°C. The liquidus temperature of the bulk weld pool, T_{LW} , is about 1422°C (1411 to 1433°C
32
33 as mentioned previously). So, $T_{LW} - T_{L2} = 337^\circ\text{C}$. Second, since the thermal conductivity of Cu is
34
35 very high, thus reducing the temperature gradients and widening the space covered by the
36
37 temperature range from T_{L2} to T_{LW} .
38
39
40
41
42

43 The very thick layer of Cu makes it very easy for the nearby liquid in the bulk weld pool
44
45 to not only intrude into it but also push much liquid Cu out into the adjacent bulk weld pool. As
46
47 can be seen in Fig. 4a, light-etching, partially mixed Cu-rich material forms a thick layer next to
48
49 the Cu-beach. A lump of light-etching Cu-rich material rests at the bottom of the bulk weld
50
51 metal, with a thick layer of partially mixed Cu above it. The composition of the lump, as
52
53 indicated by EDS, was Cu with 2 to 3 wt% Fe.
54
55
56
57

58 **4. Layered bulk weld metal**

59
60
61
62
63
64
65

1
2
3
4 As shown by the optical macrograph in Fig. 4a, the bulk weld metal exhibits a layered
5
6 structure. Although the two macrosegregation mechanisms discussed above are the main focus of
7
8 the present study on dissimilar-metal welding, this layered structure of the bulk weld metal still
9
10 needs to be discussed.
11
12

13
14 To help explain the layered structure, the Cu-Fe phase diagram in Fig. 6 was calculated
15
16 using the thermodynamic software package Pandat [35] and database PanIron of CompuTherm,
17
18 LLC [36]. The dotted curved line shortly below the equilibrium liquidus line is the metastable
19
20 miscibility gap. As mentioned previously, the bulk fusion zone contained significantly more Cu
21
22 than steel. Thus, the bulk weld pool (*a*) can have composition closer to the Cu side of the phase
23
24 diagram, for instance, Point *a*. Thus, if the bulk weld pool is undercooled into the miscibility gap
25
26 during welding, the undercooled bulk weld pool (*b*) can separate into a Cu-rich liquid phase (*c*)
27
28 and a Fe-rich liquid phase (*d*). Assuming the lever-arm rule, the fraction of the Cu-rich liquid
29
30 phase is $\frac{bd}{cd}$, and that of the Fe-rich phase $\frac{cb}{cd}$. Since the $\frac{bd}{cd}$ is much larger than $\frac{cb}{cd}$, the Cu-
31
32 rich liquid phase (*c*) can be the matrix and the Fe-rich phase (*d*) spheres in the matrix. This
33
34 primary separation can be expressed as follows: undercooled bulk weld pool (*b*) → Cu-rich
35
36 liquid matrix (*c*) + Fe-rich liquid spheres (*d*).
37
38
39
40
41
42

43
44 Besides primary separation, secondary separation of a Cu-rich liquid from inside the Fe-
45
46 rich liquid spheres can also occur. Upon further cooling, the Fe-rich liquid spheres (*d*) can
47
48 become supersaturated in Cu at Point *e* if Cu diffusion is too slow to let the Fe-rich liquid
49
50 spheres (*d*) follow the miscibility gap closely to Point *g*. This Cu supersaturation can cause Cu-
51
52 rich liquid droplets (*f*) to form from inside the Fe-rich liquid spheres (*e*). This secondary
53
54 separation can be expressed as follows: supersaturated Fe-rich liquid spheres (*e*) → Cu-rich
55
56 liquid droplets (*f*) + Fe-rich liquid spheres (*g*).
57
58
59
60
61
62

1
2
3
4
5
6
7 Lu et al. [37] studied the solidification structure of undercooled Cu-Fe melts. They
8
9 induction-melted 8 grams of alloy Cu-50Fe by at% (or Cu-46Fe by wt%) in a flux consisting of
10
11 70% Na₂SiO₃ + 17.73% Na₂B₄O₇ + 12.27% B₂O₃, which let the alloy melt to undercool below
12
13 the liquidus temperature before solidification started. One undercooled melt solidified into a
14
15 single layer consisting of Fe-rich spheres dispersed in a Cu-rich matrix. Besides this primary
16
17 separation, secondary separation of Cu-rich liquid droplets from inside the Fe-rich liquid spheres
18
19 was also observed.
20
21
22

23
24 Based on the lower density of Fe (7.86 g/cc) than Cu (8.96 g/cc), the Fe-rich liquid
25
26 spheres can be expected to be lighter than the surrounding Cu-rich liquid phase and thus float
27
28 upward to the top of the Cu-rich liquid phase. As shown by the Cu-Fe phase diagram in Fig. 6,
29
30 the liquidus line is higher in temperature on the Fe-rich side than the Cu-rich side. This suggests
31
32 the Fe-rich liquid phase has a larger local undercooling for a given bulk undercooling and hence
33
34 a larger driving force to nucleate and solidify first [37].
35
36
37

38
39 Several different factors might be related to the formation of the layered structure of the
40
41 weld metal in Fig. 4a. First, the top of the metastable miscibility gap of the Cu-Fe phase diagram
42
43 is only slightly below the liquidus line, so not much supercooling is needed for the weld pool to
44
45 enter the gap. Second, the cooling rate is fairly fast in arc welding (faster than in casting), fast
46
47 enough for the bulk weld pool to undercool into the miscibility gap to cause primary separation
48
49 of Fe-rich liquid spheres from the Cu-rich liquid matrix. The spheres are lighter than the
50
51 surrounding Cu-rich liquid and can thus float up to its top. Third, the undercooled weld pool
52
53 could have become significantly more viscous to resist mixing. Viscosity measurements have
54
55 indicated that liquid metals (and not just glass) become significantly more viscous when
56
57
58
59
60
61
62
63
64
65

1
2
3
4 undercooled [38, 39]. Fourth, horizontal rotational flow can occur in a thin weld pool with an
5
6 asymmetric current path through the pool [40, 41]. In the present study, asymmetry might be
7
8 promoted by the electrode offset to the Cu side and the much higher electrical conductivity of Cu
9
10 than steel. Horizontal rotational flow can stir the viscous bulk weld pool of low depth/width ratio
11
12 into a layered structure with one layer more or less on top of another, that is, with layers more
13
14 horizontal than vertical. Each layer can consist of a Cu-rich liquid matrix with Fe-rich liquid
15
16 spheres at the top.
17
18
19
20

21 **5. Microstructure of weld metal**

22
23 A series of SEM images of the weld is shown in Fig. 7, with their locations indicated in
24
25 Fig. 7a. It should be pointed out that Points *b* through *f* in Fig. 7a have nothing to do with Points
26
27 *b* through *f* in Fig. 6. Fig. 7b shows the solidification microstructure of the liquid that intrude
28
29 from the bulk weld pool into the Cu-rich layer at Point *b*. The microstructure consists of very
30
31 small Fe-rich spheres in a Cu-rich matrix. For comparison, Fig. 7c shows the microstructure of
32
33 the bulk weld pool nearby at Point *c* just outside the intruded area. The compositions at these two
34
35 locations are similar (close to Cu-30Fe according to Fig. 5), but the solidification microstructure
36
37 is much finer at Point *b* than at Point *c*. It is well known that the solidification microstructure
38
39 is finer at a higher cooling rate [42]. Thus, the much finer solidification microstructure at Point *b*
40
41 suggests quick freezing of the liquid intruding into the cooler layer of Cu from the bulk weld
42
43 pool. According to heat flow in welding [34], the cooling rate is lower at a point farther away
44
45 from the heat source. Thus, the cooling rate should have been lower at Point *b* than at Point *c*.
46
47 This further suggests that the higher cooling rate at Point *b* was caused by quick freezing. It is
48
49 worth mentioning that Kou and Yang [25] used a Cu-30Ni filler metal in gas-metal arc welding
50
51 of pure Cu. The liquid from the bulk weld pool was pushed by convection into the layer of
52
53
54
55
56
57
58
59
60
61
62
63
64
65

1
2
3
4 melted but unmixed Cu to freeze quickly as weld-metal intrusions in the pure-Cu beach. The
5
6 solidification microstructure was much finer in the intrusions than in the nearby bulk weld metal,
7
8 confirming fast freezing of the intrusion.
9

10
11 Consider the microstructure at Point *d* in Fig. 7a. For convenience of discussion the layer
12
13 below Point *d* will be called the lower layer, the layer above it (all the way to the weld top
14
15 surface) the upper layer, and the boundary between the two layers the interface. As can be seen
16
17 in Fig. 7a, dark dots appear to accumulate along the top of the lower layer. As will be shown
18
19 subsequently, these dark dots are Fe-rich spheres and the material between the dots is the Cu-rich
20
21 matrix. As mentioned previously, during welding the lighter Fe-rich liquid spheres can float
22
23 upward to the top of the Cu-rich liquid matrix and accumulate along the interface. Lu et al. [37]
24
25 also showed Fe-rich spheres floating up to the top of the Cu-rich layer.
26
27
28
29

30
31 Figure 7d shows a SEM image taken at Point *d*. The Fe-rich spheres at the top of the
32
33 lower layer appear more or less round and about 10 μm in diameter, with visible Cu-rich
34
35 particles inside. The composition measurements by EDS are shown in Fig. 8. Fig. 8a confirms
36
37 these spheres are Fe-rich and the particles inside are Cu-rich. The Fe-rich spheres consist of a Fe-
38
39 rich matrix (about 70 wt% Fe at Point 4) and Cu-rich particles (about 7 wt% Fe at Point 3). As
40
41 shown in Fig. 8b, the Fe-rich spheres are surrounded by a Cu-rich phase (about 7 wt% Fe at
42
43 Points 2 and 5), thus indicating Fe-rich liquid spheres floated up to the top of the Cu-rich liquid.
44
45 As mentioned previously, slow Cu diffusion can cause the Fe-rich liquid spheres to become
46
47 supersaturated with Cu during cooling, thus causing Cu-rich liquid droplets to form inside the
48
49 Fe-rich liquid spheres (secondary separation). As can be seen in Fig. 7d, the Fe-rich dendrites in
50
51 the upper layer appear to grow (upward) epitaxially from the Fe-rich spheres at the top of the
52
53 lower layer.
54
55
56
57
58
59
60
61
62
63
64
65

1
2
3
4 Now consider the microstructure at Point *e* in Fig. 7a. Again, the dark dots are Fe-rich
5
6 spheres and the material between the dots is the Cu-rich matrix. Fig. 7e shows the SEM image at
7
8 Point *e*. Numerous Fe-rich spheres about 5 to 8 μm in diameter are visible, with fine Cu-rich
9
10 particles inside. Since the Fe-rich liquid spheres are lighter than the surrounding Cu-rich liquid,
11
12 they can float upward during welding.
13
14

15
16 As for the microstructure at Point *f* in Fig. 7a, the dark dots at the top of the lower layer
17
18 are again Fe-rich spheres and the material between the dots is the Cu-rich matrix. These spheres
19
20 can be seen in the left half of the SEM image shown in Fig. 7f. During welding the lighter Fe-
21
22 rich liquid spheres floated up to the top of the lower layer. These Fe-rich liquid spheres appear to
23
24 have coalesced and contain few Cu-rich particles, suggesting a slower local cooling rate. Again,
25
26 Fe-rich dendrites in the upper layer appear to grow epitaxially from the Fe-rich spheres.
27
28

29
30 The line composition measurements in Fig. 5 show peaks of the Fe-content at locations
31
32 where the line intersects the dark dots, as indicated by vertical dotted lines 3, 4 and 5. These
33
34 peaks further confirm the dark dots are Fe-rich spheres.
35
36

37
38 The peninsula and its surroundings have already been shown previously in Fig. 4c. Some
39
40 Fe-rich liquid spheres floated upward and were stopped by the steel peninsula. Growth of
41
42 dendrites from the peninsula suggests the melted steel solidified into the peninsula before the
43
44 surrounding liquid in the bulk weld metal did, consistent with the latter being cooler and causing
45
46 the former to freeze quickly.
47
48

49
50 Figure 9 briefly summarizes the discussion so far on macrosegregation in the dissimilar-
51
52 metal weld between steel (metal 1) and Cu (metal 2). Fig. 9a shows the formation of the steel
53
54 peninsula by Mechanism I under the condition of $T_{LW} < T_{LI}$ and the formation of the irregular Cu
55
56 beach by Mechanism II under the condition of $T_{LW} > T_{L2}$. In the former, the downward flow
57
58
59
60
61

1
2
3
4 needs to be backward as well in order to carry the melted steel backward into the cooler ($T < T_{Li}$)
5
6 region ahead of the solidification front to freeze quickly. In the latter, however, the flow only
7
8 needs to be toward the pool boundary. The two mechanisms can be applied to other dissimilar-
9
10 metal welding in general, such as steel to stainless steel.
11
12

13
14 The formation of the layered structure summarized in Fig. 9b is related specifically to
15
16 butt arc welding a thin Cu sheet to a thin steel (or stainless steel) sheet. The bulk weld pool can
17
18 undercool into the metastable miscibility gap of the Cu-Fe phase diagram to form a Fe-rich
19
20 liquid phase and a Cu-rich liquid phase, the former as spheres and the latter as the matrix. Since
21
22 the Fe-rich liquid is lighter than the Cu-rich liquid, the Fe-rich spheres float upward to the top of
23
24 the Cu-rich liquid. The undercooled bulk weld pool, which is likely viscous, can be stirred by
25
26 horizontal rotational flow into a layered structure with Fe-rich spheres at the top of each Cu-rich
27
28 layer.
29
30
31

32 33 **6. Macrosegregation in laser- and electron-beam welds**

34
35 The above discussion on macrosegregation in the arc weld can help explain
36
37 macrosegregation in laser- and electron-beam welding of Cu to steel (or Fe or stainless steel) [2,
38
39 5, 8]. The latter can be difficult to understand because fluid flow can be complex in keyhole
40
41 laser- and electron-beam welding.
42
43
44

45
46 First, the existence of very small beaches, peninsulas and islands of steel (or Fe or
47
48 stainless steel) in the welds can be explained. In keyhole laser- or electron-beam welding of Cu
49
50 to steel (metal 1), the condition of $T_{LW} < T_{Li}$ for the formation of beaches, peninsulas and small
51
52 islands of unmixed steel also exists. However, these features can be expected to be very small
53
54 because the layer of unmelted steel tends to be very thin in laser- or electron-beam welding due
55
56
57
58
59
60
61
62
63
64
65

1
2
3
4 to the very narrow weld pool and very strong convection in the pool. These small
5
6
7 macrosegregation features are often not noticed.

8
9 Second, the existence of relatively thick beaches of unmixed Cu [2, 7] and irregular-
10
11 shaped Cu or Cu-rich beaches [1, 2, 5, 8-10] can also be explained. In keyhole laser- or electron-
12
13 beam welding of Cu (metal 2) to steel, the condition of $T_{LW} > T_{L2}$ for the formation of irregular-
14
15 shaped beaches or islands of unmixed Cu also exists. Due to $T_{LW} \gg T_{L2}$ and the very high Cu
16
17 thermal conductivity, the layer of unmixed liquid Cu can still be expected to be relatively thick,
18
19 though thinner than that in arc welding because of the narrow weld pool and strong convection in
20
21 laser- and electron-beam welding.
22
23
24

25
26 Third, the existence of the unusually large Cu-rich islands of irregular shape in the bulk
27
28 weld metal near the Cu side [1, 2, 5, 7-10] and even far away from it [1, 7, 8] can also be
29
30 explained. Since the cooling rate is very fast in laser- and electron-beam welding, the bulk weld
31
32 pool itself solidifies rapidly. Thus, the liquid Cu carried into the bulk weld pool, even if it is
33
34 unusually large, can also solidify quickly with limited mixing with the bulk weld pool.
35
36
37

38
39 Finally, the existence of a layered structure that is more vertical than horizontal in the
40
41 bulk weld metal can also be explained [1, 5, 7-9]. Under the very high cooling rate in keyhole
42
43 laser- or electron-beam welding, the weld pool can easily undercool into the miscibility gap of
44
45 the Cu-Fe phase diagram to form two immiscible liquid layers. As mentioned previously, the
46
47 viscosity of a liquid metal can increase significantly with increasing undercooling. Thus, the
48
49 undercooled weld pool may be viscous to promote the formation of a layered structure in the
50
51 weld pool. The high cooling rate can help the layered liquids solidify before being dispersed. The
52
53 depth/width ratio of the weld pool is much greater in keyhole laser- and electron-beam welding
54
55 than in arc welding. Thus, as compared to arc welding of thin sheets (Fig. 4a), the flow loop in
56
57
58
59
60
61
62
63
64
65

1
2
3
4 the weld pool can be more vertical even near the top surface of the weld pool, where the loop can
5
6 be shallower due to influence by flow driven by surface-tension gradients. The layered structure
7
8 often showed relatively thick Cu-rich bands near the weld top surface on the Cu side, where
9
10 melting of Cu was most intensive. It is interesting that an onion-ring structure, wider in the
11
12 vertical direction than horizontal, was observed deep below the weld top surface [5]. As in arc
13
14 welding, spheres of one phase in the matrix of another can be expected and, in fact, have been
15
16 observed [1, 2, 5, 8-10].
17
18
19
20

21 **7. Welding stainless steels dissimilar in sulfur content**

22
23 A 304L stainless steel with 0.003 wt% S has been butt welded to a 303 stainless steel
24
25 with 0.293 wt% S, both with about 18 wt% Cr and 8 wt% Ni [42-44]. It was observed in both
26
27 gas-tungsten arc welding and conduction-mode laser-beam welding that the low-S stainless steel
28
29 (304L) melted to a significantly greater extent than the high-S one (303). Sulfur, S, is known to
30
31 be a surface-active agent in steels and stainless steels. Increasing the S content can change $d\gamma/dT$
32
33 from negative to positive and hence reverse the direction of surface-tension driven flow, where γ
34
35 is surface tension and T temperature [34]. Detailed computer simulation of heat transfer, fluid
36
37 flow and mass transfer was conducted. The lateral shift of the weld pool from the original joint
38
39 interface (toward the low-S one) and the rotation of the weld pool at an angle with the interface
40
41 were both explained. Since the liquidus temperature is hardly affected by S at these low
42
43 concentration levels, the special situation of $T_{LW} = T_{L1} = T_{L2}$ can exist. However, since both
44
45 stainless steels contained about 18 wt% Cr and 8 wt% Ni, no significant macrosegregation of Cr
46
47 or Ni was observed. For significant macrosegregation to occur, the two materials needs to differ
48
49 significantly in the contents of major alloying elements (such as Cr and Ni) and hence in the
50
51 liquidus temperature as explained in the present study.
52
53
54
55
56
57
58
59
60
61
62
63
64
65

1
2
3
4
5 **Conclusions**
6
7

- 8 1. Two mechanisms of macrosegregation in dissimilar-metal fusion welding have been
9 proposed to explain the formation of macrosegregation features based on the liquidus
10 temperature of the bulk weld metal T_{LW} relative to those of metal 1 (or alloy 1) T_{L1} and
11 metal 2 (or alloy 2) T_{L2} .
12
13 2. Mechanism 1 is for the case of $T_{LW} < T_{L1}$, and it can explain the formation of peninsulas
14 or islands as well as beaches of unmixed metal 1.
15
16 3. Mechanism 2 is for the case of $T_{LW} > T_{L2}$, and it can explain why the beaches of unmixed
17 metal 2 can form with an irregular shape.
18
19 4. These two mechanisms have been verified in arc welding of Cu (metal 2) to steel (metal
20 1) by the formation of a peninsula of unmixed steel and an irregular-shaped beach of
21 unmixed Cu. A thick liquid layer of unmixed Cu can exist next to Cu because of two
22 reasons: (i) the much lower melting point of Cu than steel, i.e., $T_{LW} \gg T_{L2}$, and (ii) the
23 very high thermal conductivity of Cu.
24
25 5. A layered structure, with layers more horizontal than vertical, has been observed in the
26 bulk weld metal. It is caused by undercooling of the bulk weld pool into a metastable
27 miscibility gap in the Cu-Fe phase diagram and possibly promoted by horizontal
28 rotational flow in the weld pool, which has a low depth/width ratio.
29
30 6. In laser- or electron-beam welding, a relatively thick liquid layer of unmixed Cu can also
31 exist next to Cu for the same reasons as in arc welding. However, when swept far away
32 by convection, liquid Cu can still solidify as large Cu-rich islands (instead of mixing into
33 the bulk weld pool) because the bulk weld pool itself can solidify very fast. A layered
34
35
36
37
38
39
40
41
42
43
44
45
46
47
48
49
50
51
52
53
54
55
56
57
58
59
60
61
62
63
64
65

1
2
3
4 structure can also form because of the same reasons as in arc welding, but more vertical
5
6 than horizontal because of the deep and narrow weld pool associated with the keyhole.
7
8
9

10 **Acknowledgements**

11
12 The authors would like to thank CompuTherm, LLC in Madison, WI for kindly providing
13
14 Pandat 2013 and PanIron 2013 for calculating the Cu-Fe phase diagram and Dr. Chuang Zhang
15
16 of CompuTherm for assistance in the miscibility gap calculation. They are grateful to Dr. John
17
18 H. Fournelle of the Department of Geoscience, UW-Madison for composition measurements by
19
20 EPMA. They would also like to thank Dr. Ping Yu for helpful discussions on the weld
21
22 microstructure. This work was supported by the National Science Foundation under Grant No.
23
24 DMR 1500367.
25
26
27
28
29

30 **References**

- 31
32 1. S. Chen, J. Huang, J. Xia, H. Zhang and X. Zhao, “Microstructural Characteristics of a
33
34 Stainless Steel/Copper dissimilar joint by laser welding”, Metallurgical and Materials
35
36 Transactions A, 44a (2013) 3690-3696.
37
38
- 39
40 2. I. Magnabosco, P. Ferro, F. Bonollo, L. Arnberg, “An investigation of fusion zone
41
42 microstructures in electron beam welding of copper–stainless steel”, Materials Science
43
44 and Engineering A 424 (2006) 163–173.
45
46
- 47
48 3. S. Asai, T. Ogawa, Y. Ishizaki, T. Minemura, H. Minami and S. Miyazaki, “Application
49
50 of plasma MIG hybrid welding to dissimilar joints between copper and steel”, **No. 02**
51
52 2012, vol. 56, Welding in the World, pp. 37-42.
53
54
55
56
57
58
59
60
61
62
63
64
65

- 1
2
3
4 4. T. A. Mai, A.C. Spowage, “Characterisation of dissimilar joints in laser welding of steel–
5 kovar, copper–steel and copper–aluminium”, *Materials Science and Engineering A* 374
6 (2004) 224–233.
7
8
- 9
10
11
12 5. G. Phanikumar, S. Manjini, P. Dutta, J. Mazumder, K. Chattopadhyay, Characterization
13 of a continuous CO₂ laser-welded Fe–Cu dissimilar couple. *Metall. Mater. Trans. A* 36
14 (2005) 2137–2147.
15
16
- 17
18
19
20 6. B. Zhang, J. Zhao, X. Li, and G. Chen, “Effects of filler wire on residual stress in
21 electron beam welded QCr0.8 copper alloy to 304 stainless steel joints”, *Applied Thermal*
22 *Engineering* 80 (2015) 261-268.
23
24
- 25
26
27
28 7. B. Zhang, J. Zhao, X. Li, J. Feng, “Electron beam welding of 304 stainless steel to
29 QCr0.8 copper alloy with Cu filler wire”, *Trans. Nonferrous Met. Soc. China* 24(2014)
30 4059–4066.
31
32
- 33
34
35
36 8. S. Chen, J. Huang, J. Xia, X. Zhao, S. Lin, “Influence of processing parameters on the
37 characteristics of stainless steel-copper laser welding”, *Journal of Materials Processing*
38 *Technology* 222 (2015) 43–51.
39
40
- 41
42
43
44 9. C. Yao, B. Xu, X. Zhang, J. Huang, J. Fu, Y. Wu, “Interface microstructure and
45 mechanical properties of laser welding copper–steel dissimilar joint”, *Optics and Lasers*
46 *in Engineering* 47 (2009) 807–814.
47
48
- 49
50
51
52 10. A. Munitz, 1995. “Metastable liquid phase separation in tungsten inert gas and electron
53 beam copper-stainless-steel welds”, *Journal of Materials Science* 30(1995) 2901-2910.
54
55
56
57
58
59
60
61
62
63
64
65

- 1
2
3
4 11. T. Doody: "Intermediate mixed zones in dissimilar metal welds for sour service,"
5
6 Welding Journal, 61: 55-60, 1992.
7
- 8
9
10 12. A. A. Omar: "Effects of welding parameters on hard zone formation at dissimilar metal
11
12 welds," Welding Journal, 67: 86s-93s, 1998.
13
14
- 15 13. R. Dehmlaei, M. Shamanian, A. Kermanpur, "Effect of electromagnetic vibration on the
16
17 unmixed zone formation in 25Cr-35Ni heat resistant steel/alloy 800 dissimilar welds",
18
19 Materials Characterization 59(2008) 1814-1817.
20
21
- 22
23 14. H. Naffakh, M. Shamanian, F. Ashrafizadeh, Journal of Materials Processing Technology
24
25 209(2009) 3628-3639.
26
27
- 28
29 15. G. E. Linnert: Welding Metallurgy, vol. 2. American Welding Society, Miami, 1967.
30
31
- 32 16. W. F. Savage, E. F. Nippes, and E. S. Szekeres: "Hydrogen induced cold cracking in a
33
34 low alloy steel," Welding Journal, 55: 276s-283s, 1976.
35
36
- 37 17. M. D. Rowe, T. W. Nelson, and J. C. Lippold: "Hydrogen-induced cracking along the
38
39 fusion boundary of dissimilar metal welds," Welding Journal, 78: 31s-37s, 1999.
40
41
- 42
43 18. H. Cordier, M. Schippers, and I. Polmear: "Microstructure and intercrystalline fracture in
44
45 a weldable aluminum-zinc-magnesium alloy," Z. Metallkde, 68: 280-284, 1977.
46
47
- 48
49 19. M. Pirner, and H. Bichsel, "Corrosion resistance of welded joints in AlZnMg," Metall,
50
51 29: 275-280, 1975.
52
53
- 54 20. W. A. Baeslack III, J. C. Lippold, and W. F. Savage: "Unmixed zone formation in
55
56 austenitic stainless steel weldments," Welding Journal, 58: 168s-176s, 1979.
57
58
- 59
60 21. K. G. Kent: Metals and Materials, "Weldable Al-Zn-Mg alloys," 4: 429-440, 1970.
61

- 1
2
3
4 22. W. F. Savage and E. S. Szekeres: "A mechanism for crack formation in HY-80 steel
5 weldments," *Welding Journal*, 46: 94s-96s, 1967.
6
7
8
9
10 23. W. F. Savage, E. F. Nippes and E. S. Szekeres: "A study of fusion boundary phenomena
11 in a low alloy steel," *Welding Journal*, 55: 260s-268s, 1976.
12
13
14
15 24. S. Kou: *Transport Phenomena and Materials Processing*, John Wiley and Sons, New
16 York, NY, 1996, pp. 57-60.
17
18
19
20 25. S. Kou and Y. K. Yang, "Fusion-Boundary Macroseggregation in Dissimilar-Filler
21 Welds", *Welding Journal*, vol. 86, 2007, pp. 303s to 312s.
22
23
24
25
26 26. Y. Yang and S. Kou, "Macroseggregation in Al-Si Welds Made with Dissimilar Filler
27 Metals", *Science and Technology of Welding and Joining*, vol. 15, No. 1, 2010, pp. 1-14.
28
29
30
31
32 27. Y. K. Yang and S. Kou, "Macroseggregation Mechanisms in Arc Welds Made with
33 Dissimilar Filler Metals", *Science and Technology of Welding and Joining*, vol. 15, No.
34 1, 2010, pp. 15-30.
35
36
37
38
39 28. Y. Yang and S. Kou, "Macroseggregation in Cu-30Ni Welds Made with Dissimilar Filler
40 Metals", *Science and Technology of Welding and Joining*, vol. 13, No. 4, 2008, pp. 318-
41 326.
42
43
44
45
46
47
48 29. Y. K. Yang and S. Kou, "Fusion-Boundary Macroseggregation in Dissimilar-Filler Al-Cu
49 Welds", *Welding Journal*, vol. 86, 2007, pp. 331s to 339s.
50
51
52
53 30. Y. K. Yang and S. Kou, "Weld-Bottom Macroseggregation Caused by Dissimilar Filler
54 Metals, *Welding Journal*, vol. 86, 2007, pp. 379s to 387s.
55
56
57
58
59
60
61
62
63
64
65

- 1
2
3
4 31. R. T. Houldcroft: "Dilution and uniformity in aluminum alloy weld beads," British
5 Welding Journal, 1: 468-472, 1954.
6
7
8
9
10 32. S. Kou and D. K. Sun: "Fluid Flow and Weld Penetration in Stationary Arc Welds",
11 Metallurgical Transactions A, vol. 16A, 1985, p. 203.
12
13
14
15 33. S. Kou and Y. H. Wang: "Computer Simulation of Convection in Moving Arc Weld
16 Pools", Metallurgical Transactions A, vol. 17A, 1986, p. 2271.
17
18
19
20
21 34. S. Kou: Welding Metallurgy, 2nd ed., Wiley, New York, NY, 2003, pp. 114, 180, 206,
22 208 and 306.
23
24
25
26 35. Pandat – Phase Diagram Calculation software package for Multicomponent Systems,
27 Computherm LLC, Madison, WI 53719, 2013.
28
29
30
31 36. PanIron – Thermodynamic database for Commercial Aluminum Alloys, Computherm
32 LLC, Madison, WI 53719, 2013.
33
34
35
36
37 37. X. Y. Lu, C. D. Cao, B. Wei, Microstructure evolution of undercooled iron–copper
38 hypoperitectic alloy, Materials Science and Engineering A313 (2001) 198–206.
39
40
41
42
43 38. P.-F. Paradis, T. Ishikawa and S. Yoda, Surface tension and viscosity of liquid and
44 undercooled tantalum measured by a containerless method", Journal of Applied Physics
45 97, 053506 (2005).
46
47
48
49
50 39. P.-F. Paradis, T. Ishikawa and S. Yoda, Viscosity of liquid undercooled tungsten, Journal
51 of Applied Physics 97, 106101 (2005).
52
53
54
55 40. R. A. Woods and D. R. Milner, Motion in the weld pool in arc welding, Welding Journal,
56 vol. 50, 1971, pp. 163s-173s.
57
58
59
60
61
62
63
64
65

- 1
2
3
4 41. W. H. S. Lawson and H. W. Kerr, Fluid motion in GTA weld pools, Part 1: flow patterns
5 and weld pool homogeneity, Welding Research International, volume 6, 1976, number 5,
6 pp. 63-77.
7
8
9
10
11
12 42. M. C. Flemings, Solidification Processing, McGraw-Hill, New York, 1974.
13
14
15 43. S. Mishra, T. J. Lienert, M. Q. Johnson, T. DebRoy, An experimental and theoretical
16 study of gas tungsten arc welding of stainless steel plates with different sulfur
17 concentrations, Acta Materialia 56 (2008) 2133–2146.
18
19
20
21
22
23 44. T. J. Lienert, P. Burgardt, K. L. Harada, R.T. Forsyth and T. DebRoy, Weld bead center
24 line shift during laser welding of austenitic stainless steels with different sulfur content,
25 Scripta Materialia 71 (2014) 37–40.
26
27
28
29
30
31 45. H. L. Wei, S. Pal, V. Manvatkar, T. J. Lienert, T. DebRoy, Asymmetry in steel welds
32 with dissimilar amounts of sulfur, Scripta Materialia 108 (2015) 88–91.
33
34
35
36

37 Figure Captions

38
39 Fig. 1 Dissimilar-filler welding concepts of Kou and Yang [25-30] (to be applied to dissimilar-
40 metal welding) showing solidification front: (a) at T_{LB} ; (b) shifted backward by dissimilar
41 filler to $T_{LW} (< T_{LB})$; (c) shifted forward by dissimilar filler to $T_{LW} (> T_{LB})$. Filler metal
42 changes composition and hence liquidus temperature of bulk weld metal. Pool boundary
43 (thick blue line) is no longer isothermal with dissimilar filler.
44
45
46
47
48
49
50

51 Fig. 2 Mechanism I for macrosegregation in dissimilar-metal welding under the condition of T_{LW}
52 $< T_{LJ}$: (a) phase diagram of Cu-Fe as an example; (b) plan view of weld pool and its
53 surroundings; (c) formation of beach alone; (d) formation of peninsula and island as well
54
55
56
57
58
59
60
61
62
63
64
65

1
2
3
4 as beach. T_{LW} is based on the measured composition of the bulk weld metal (shown
5
6 subsequently in Fig. 5).
7

8
9 Fig. 3 Mechanism II for macrosegregation in dissimilar-metal welding under the condition of
10
11 $T_{LW} > T_{L2}$: (a) phase diagram of Cu-Fe as an example; (b) plan view of weld pool and its
12
13 surroundings; (c) formation of smooth beach; (d) formation of beach of irregular shape.
14
15

16 Fig. 4 Transverse macrograph of Cu-to-steel arc weld: (a) overall structure; (b) fusion boundary
17
18 (indicated by arrowheads) on Cu side and Cu beach of irregular shape; (c) steel peninsula
19
20 and its surrounding microstructure.
21
22

23 Fig. 5 Composition measurements by EPMA at various locations inside the weld and along a
24
25 horizontal straight line across the weld. The peak Fe contents at lines 3, 4 and 5 are
26
27 associated with the intersections between the horizontal straight line and dark dots (Fe-
28
29 rich spheres).
30
31

32 Fig. 6 Cu-Fe phase diagram calculated using thermodynamic software Pandat [35] and database
33
34 PanIron [36] of CompuTherm, LLC. Primary separation: undercooled bulk weld pool (b)
35
36 \rightarrow Cu-rich matrix (c) + Fe-rich spheres (d). Secondary separation: Fe-rich spheres
37
38 supersaturated with Cu (e) \rightarrow Cu-rich liquid droplets (f) + Fe-rich spheres (g).
39
40
41
42

43 Fig. 7 Microstructure of Cu-steel arc weld: (a) optical micrograph showing locations of SEM
44
45 images in fusion zone; (b) - (f) SEM images.
46
47

48 Fig. 8 SEM image in Fig. 7d (Point d) enlarged: (a) composition measurements by EDS; (b)
49
50 schematic sketch of microstructure around Points 3 through 5 during welding.
51
52

53 Fig. 9 Summary of segregation features in dissimilar-metal welding revealed with the help of arc
54
55 welding Cu (metal 2) to steel (metal 1): (a) formation of peninsula under the condition of
56
57
58
59
60
61
62
63
64
65

1
2
3
4 $T_{LW} < T_{L1}$ and irregular beach under $T_{LW} > T_{L2}$; (b) formation of layered weld-metal
5
6
7 structure.
8
9
10
11
12
13
14
15
16
17
18
19
20
21
22
23
24
25
26
27
28
29
30
31
32
33
34
35
36
37
38
39
40
41
42
43
44
45
46
47
48
49
50
51
52
53
54
55
56
57
58
59
60
61
62
63
64
65

Figure(s)
Figure 1

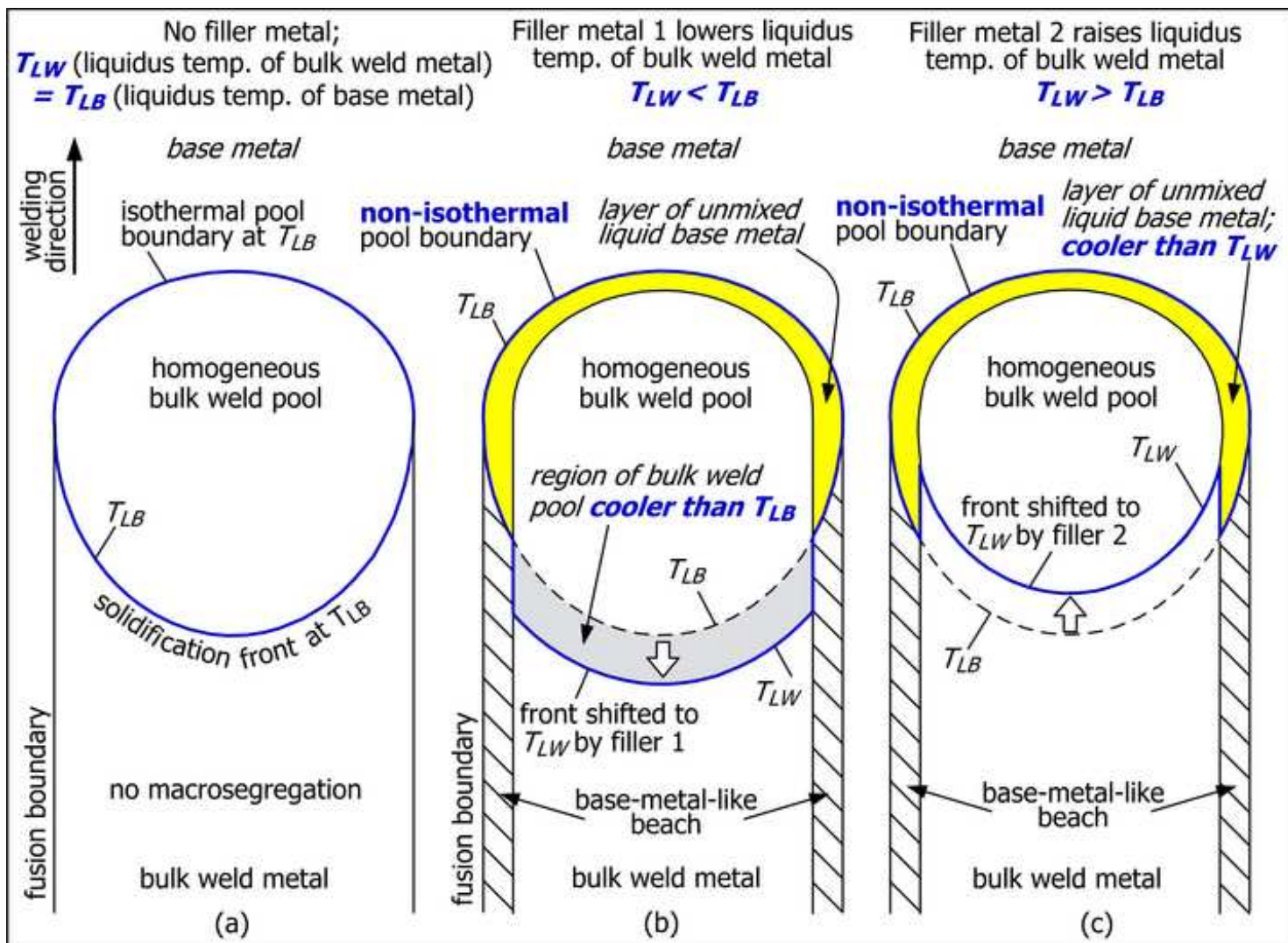


Figure 2

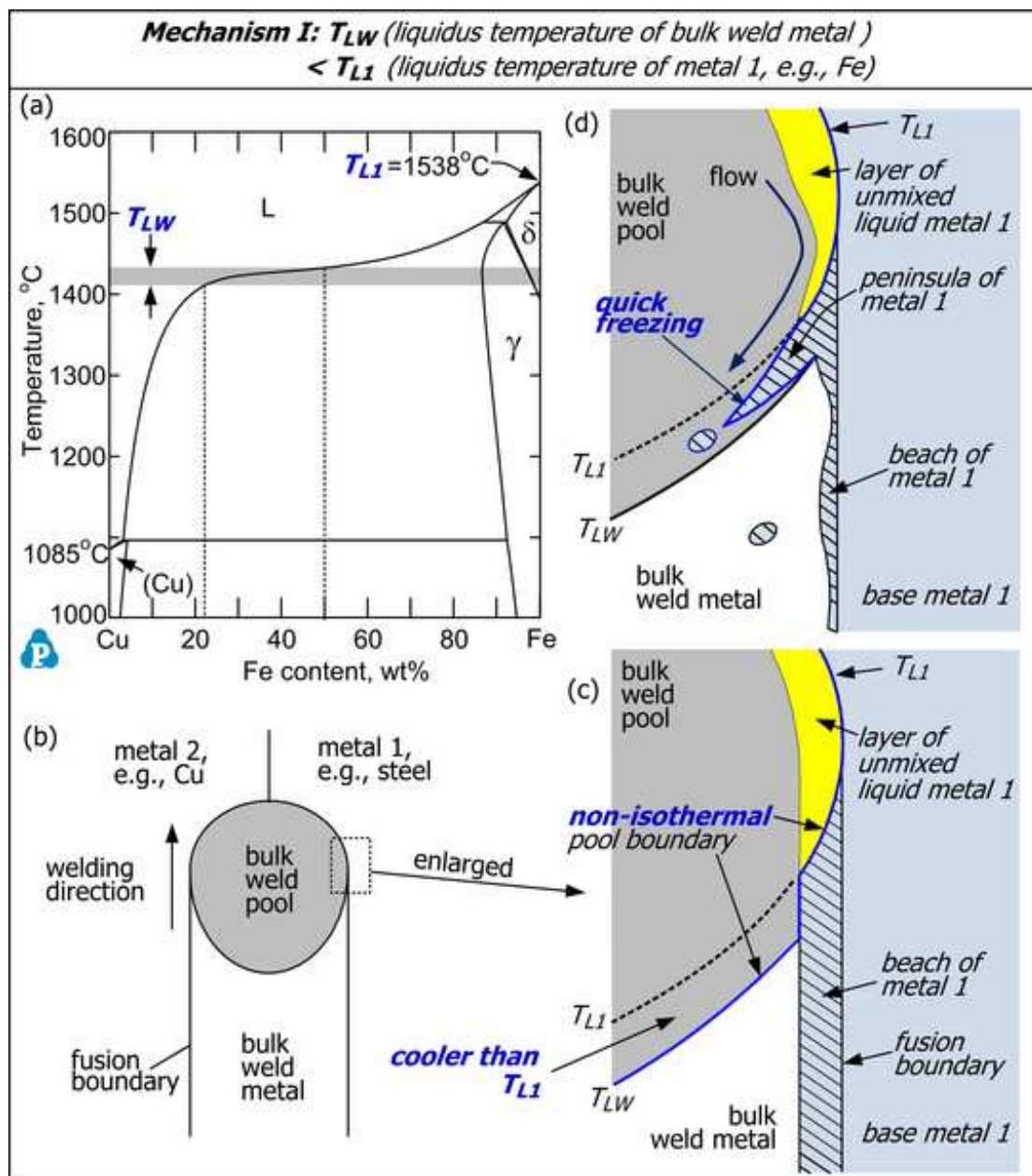


Figure 3

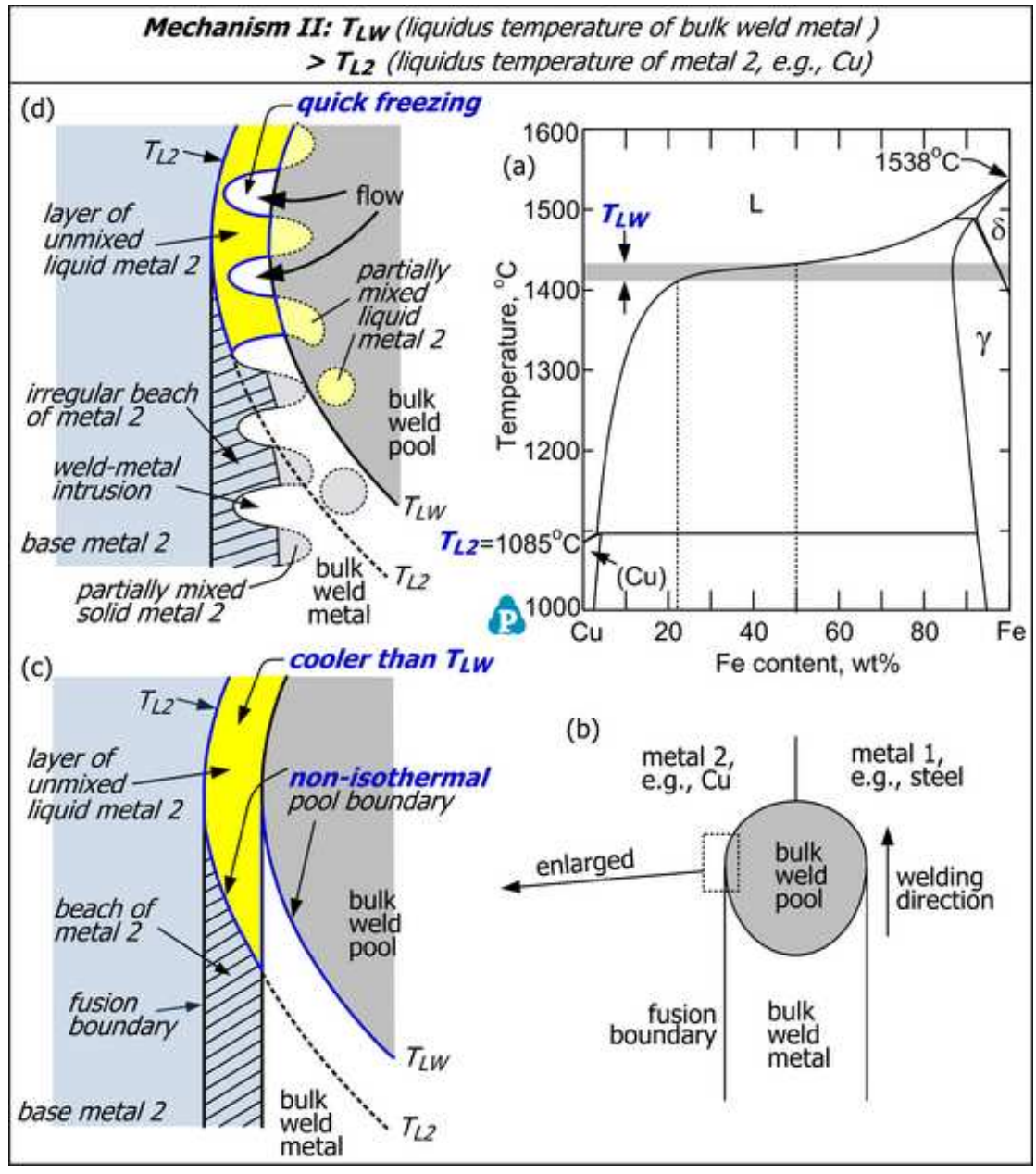


Figure 4

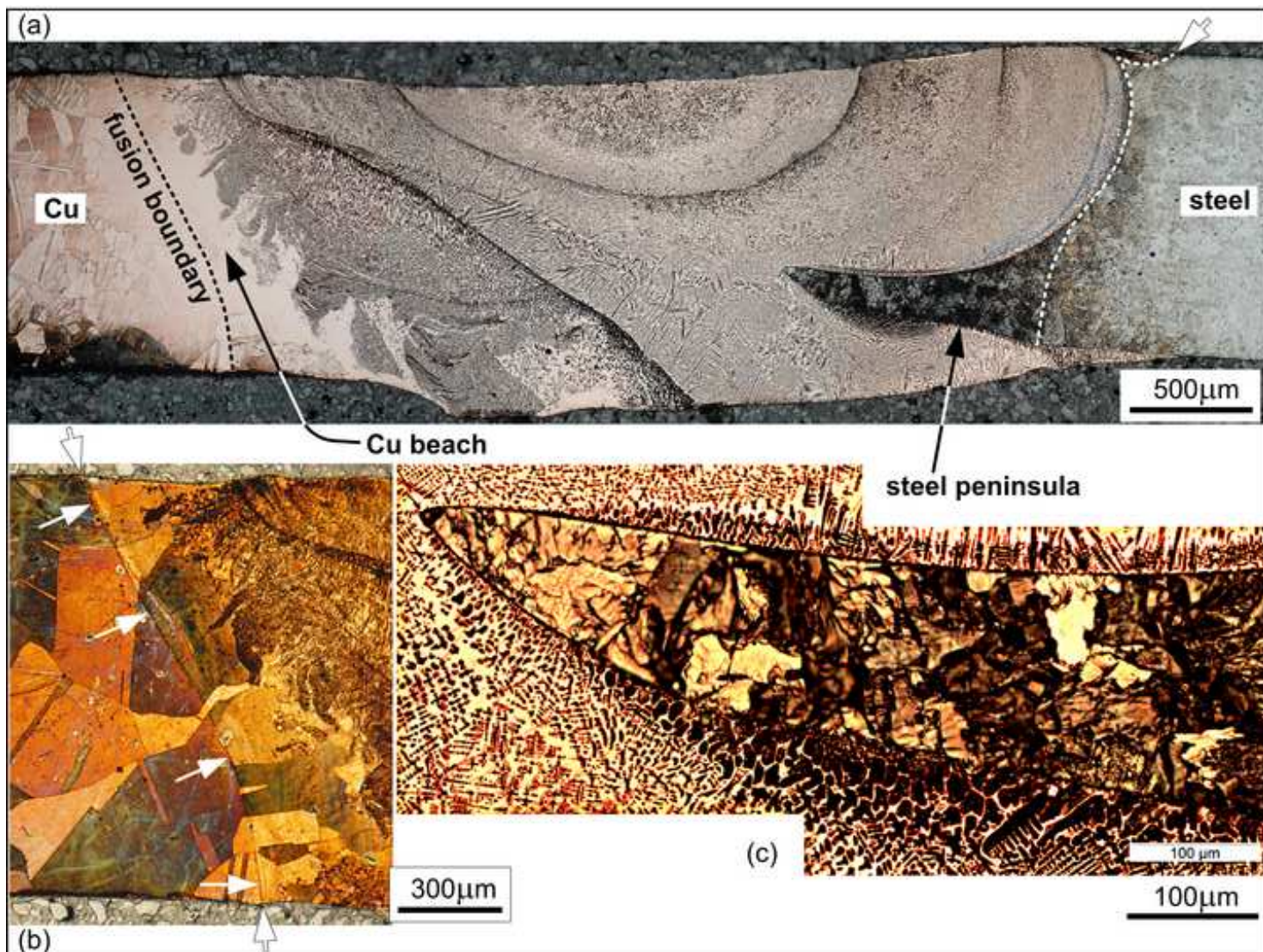


Figure 5

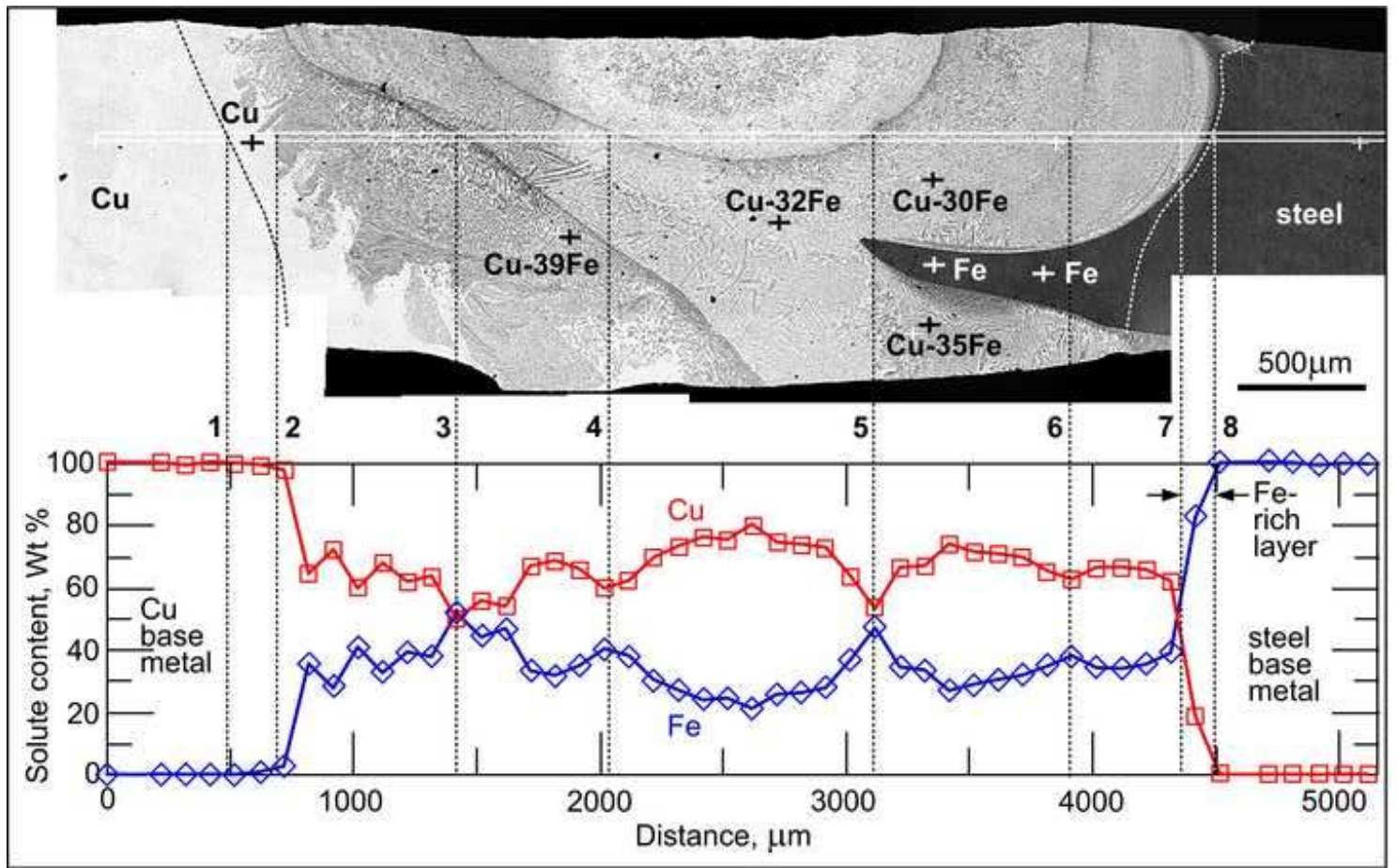


Figure 6

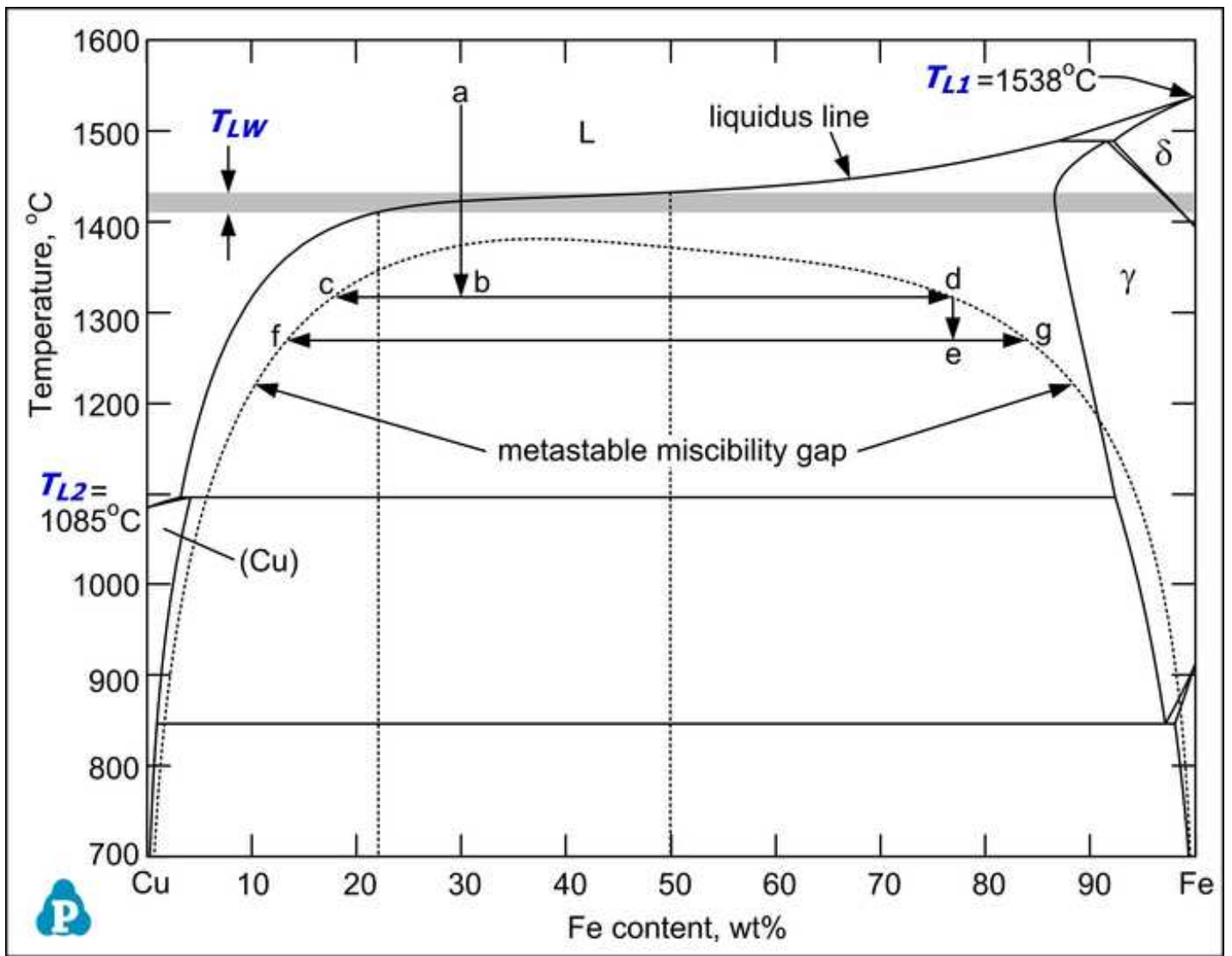


Figure 7

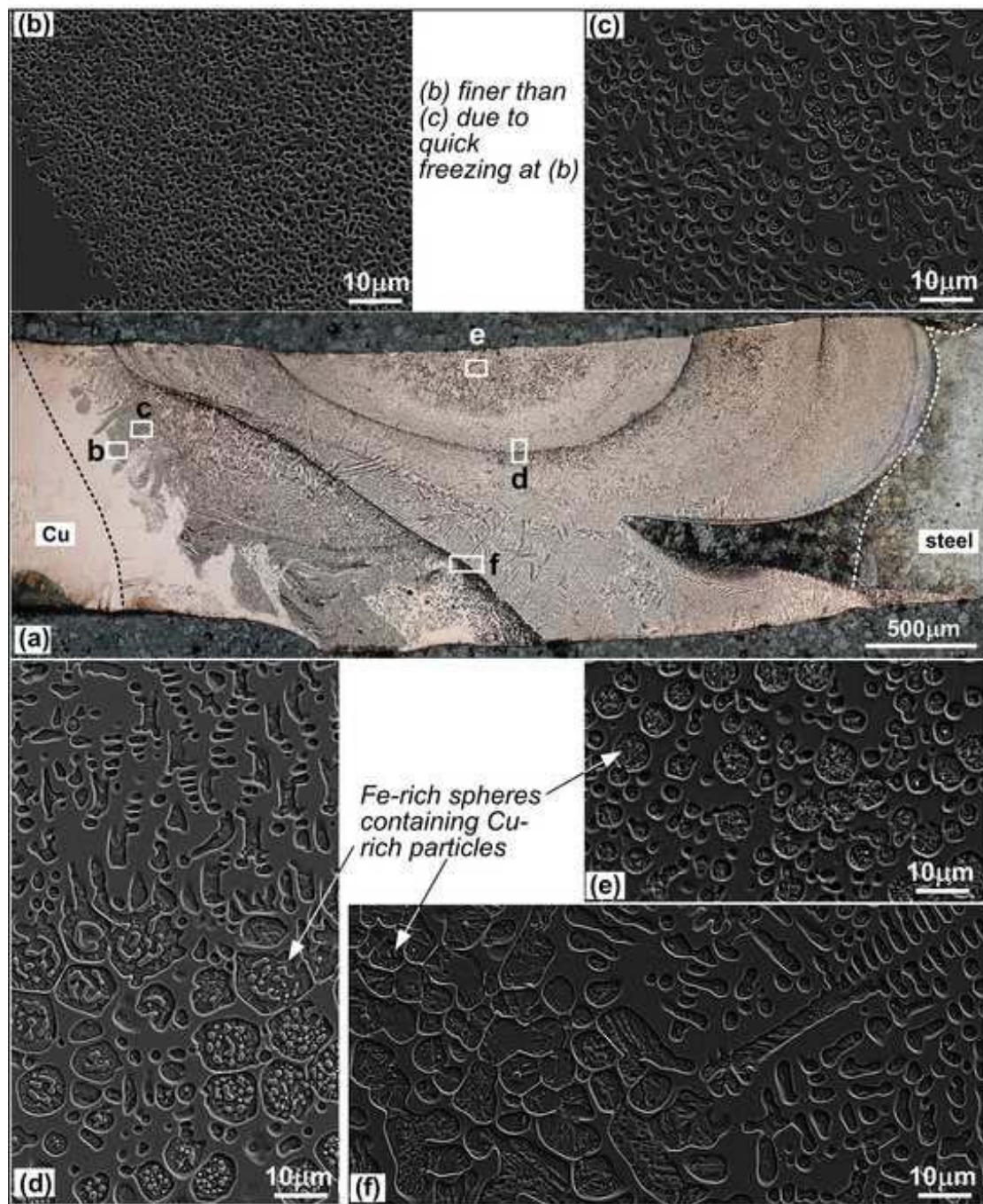


Figure 8

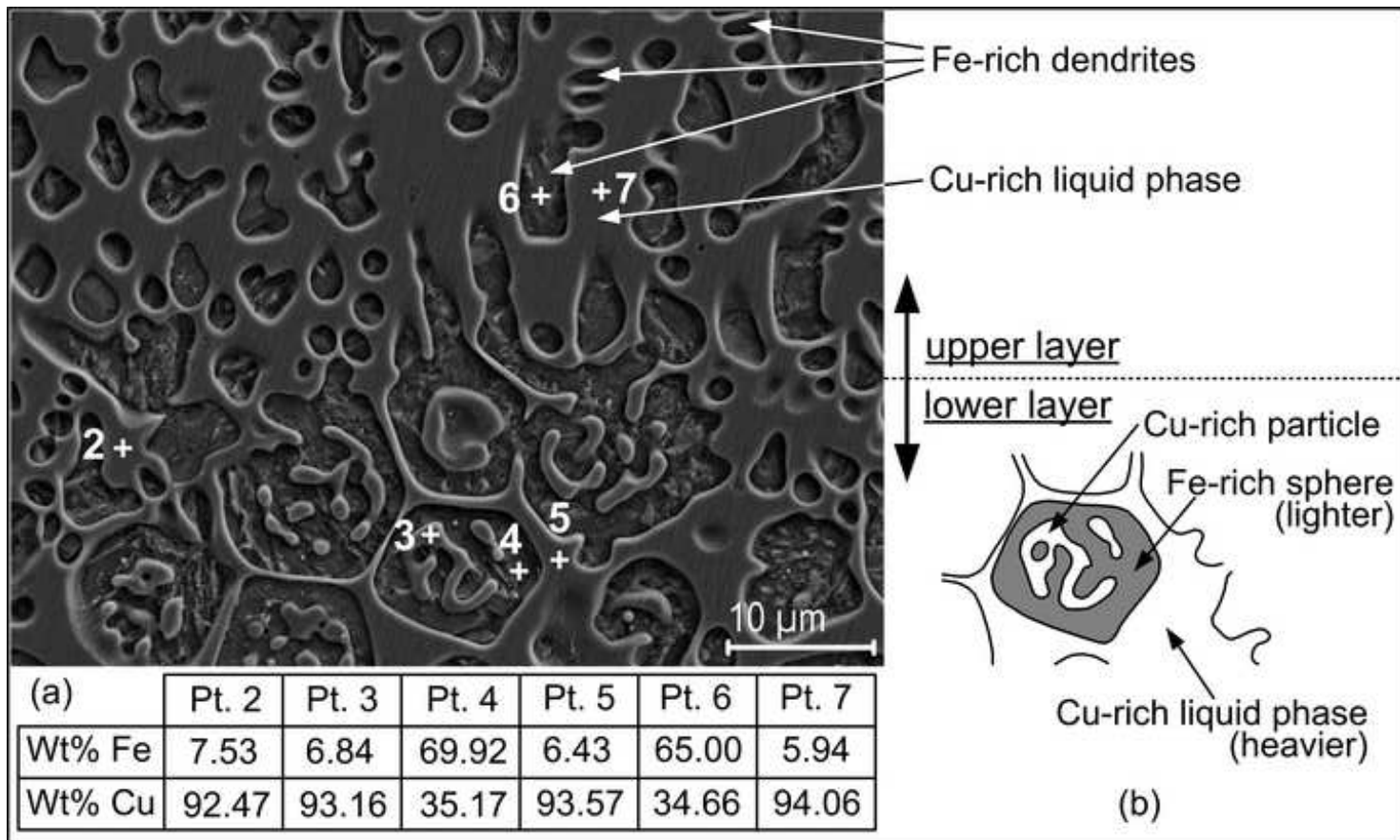
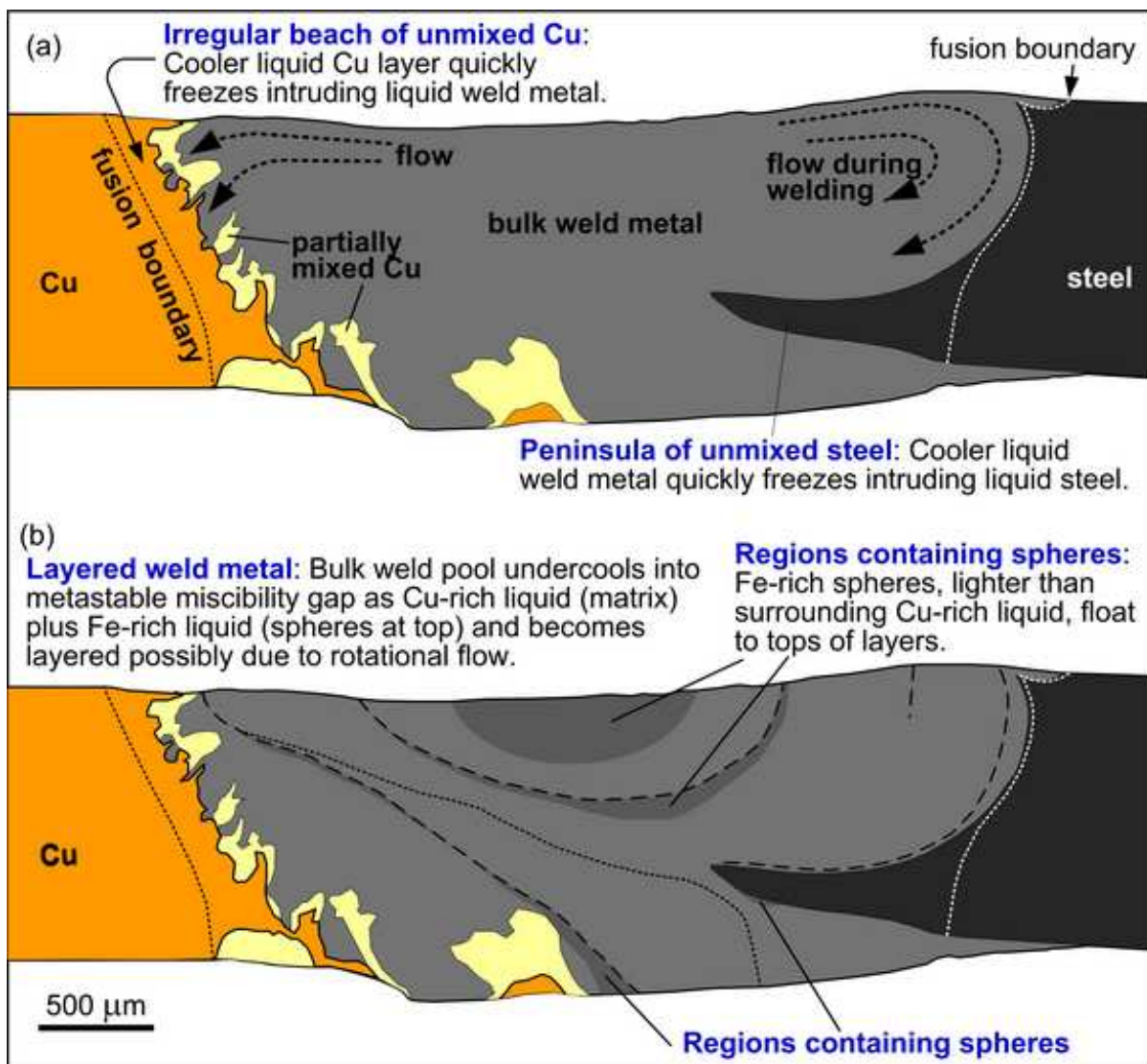
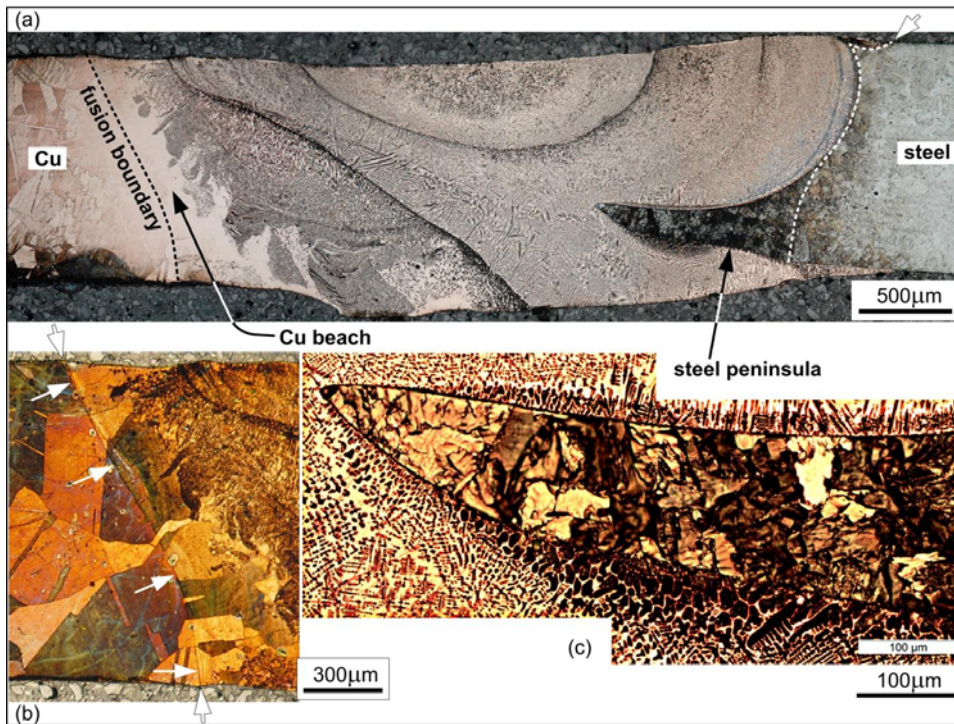


Figure 9



Graphic Abstract Solute segregation across a weld between two dissimilar metals or alloys has long been recognized, but fundamental understanding is still lacking. Two macrosegregation mechanisms were proposed based on the liquidus temperature of the bulk weld metal T_{LW} relative to those of metal 1 (or alloy 1) T_{L1} and metal 2 (or alloy 2) T_{L2} . A “peninsula” of an unmixed metal 1 can form if $T_{LW} < T_{L1}$, while a “beach” of unmixed metal 2 irregular in shape can form if $T_{LW} > T_{L2}$. The mechanisms were verified in Cu-to-steel arc welding. The bulk weld metal showed a layered structure caused by undercooling of the bulk weld pool into a metastable miscibility gap in the Cu-Fe phase diagram. These findings were used to explain macrosegregation observed in laser- and electron-beam welding of Cu to steel or stainless steel.



Transverse macrograph of Cu-to-steel arc weld showing three macrosegregation features: a steel peninsula (right), an irregular-shape Cu beach (left) and a layered weld metal (bulk fusion zone).